Comparative Study of an Electro Seismic Investigation of the TH10 geothermal well located on the Tauhara Geothermal system near Taupo, NZ

M. Du Preez,[1] J.R. McKendry[2]

[1] *ATS, 11 Jac van Rhyn St, Universitas, Bloemfontein, 9301, South Africa*
[2] *Geothermal Mapping Ltd., 26 Emily St, Gisbourne, 4010 , New Zealand*
3
4
5
6

Abstract

The TH10 geothermal well site in the Tauhara Geothermal System located near the town of Taupo in New Zealand was chosen for an Electro Seismic comparative study. The aim of the study is to determine the effectiveness of electro seismic geophysical methods on evaluating aquifer permeability in deep earth geothermal systems. In order to achieve this, a grid of electro seismic soundings were done on a blind test site around the vertically drilled TH10 geothermal well. This electro seismic data was analysed using the ATS Geothermal GeoSuite tools, for aquifer permeability tomography, electro seismic coupling coefficient tomography, geological interface tomography and geological fracturing tomography. An interpretation of the depth of the main permeable aquifers around the TH10 well was completed. This data was then compared to the known geological, hydrological, lithological, temperature and pressure data for the TH10 geothermal well. There is a good correlation between the interpreted electro seismic permeable levels and the known permeable levels in the TH10 well, interpreted from pressure, temperature and fluid velocity profiles by the owners of the well, Contact Energy, prior to the blind study. The correlation is good for both the shallow aquifers and deep ones to a depth of 2326m. A tool for predicting temperature from the electro seismic results was developed using the known temperature profile and will be subjected to further testing.

Key words: Geothermal, Electro seismic, Electro kinetic, TH10, Permeability, Electro seismic coupling coefficient, Electro seismic interface tomography, Electro Seismic fracture tomography, Tauhara.

1 Introduction

1.1 Background[22]

The first work done that contributed to the development of the electro-seismic effect was done in 1944 by Frenkel[23]. He described the relative flow of fluid to the matrix brought about by the passage of a compression seismic wave relationship. In 1962, Biot[26] made further progress by developing theories that predicted movement of a seismic wave through a saturated porous media. Various advances toward the development of a general equation describing the link between the relative fluid matrix interaction, and the electro-magnetic fields induced by this motion, were formulated between 1962[26] and 1994[16].

These developments include irreversible thermodynamic coupling effects in porous media and averaging of fluid volume to determine the governing equations of the electro seismic effect. Then in 1996, Haartsen and Pride[17] explained the electromagnetic field induced by the fluid motion relative to a porous matrix as being generated by dynamic current imbalances. These current imbalances are generated by plane shear waves moving across an interface between rocks with different electro seismic properties. These net current imbalances induce an electromagnetic field which can be read at the surface as an interface response. However, if the plane shear waves pass through a homogeneous saturated medium with no interfaces of different electro kinetic properties then the net currents induced will be balanced and cancel each other out. This essentially means there is no current flow induced by the relative motion of the fluid and matrix. This means no electromagnetic fields are induced that can be read at the surface. In 1996 Haartsen and Pride[17] made use of their findings on electromagnetic interface response to investigate electro kinetic waves from single point sources in layered rock formations. They discovered saturated media interfaces produced a response equivalent to that of a dipole induced field on the interface directly under the seismic point source. In 1981, Chandler[28] used a theoretical model and saturated core samples in laboratory experiments to relate the rise time of electro seismic signals to permeability. However, Haartsen, et al[9] in 1998 proved that the electro seismic response is a function of the salinity, porosity and permeability of a porous elastic media.

1.2 The electric double layer[6]

The works of Du Preez,2005[22] and Fourie, 2000[6] show that grains of rock display net electric charges on their surfaces due to unsatisfied chemical bonds. In an aquifer, water makes contact with these charged surfaces and an electric potential is produced, since water is also electrolytic in nature. This potential difference then draws the free ions in the water toward the surface of the grain of rock where an electric double layer is formed. An electric double layer consists of a layer of ions drawn into the solid surface by electrostatic Van der Waal forces. This inner layer is called the Stern layer, while the outer layer consists of free ions in the water drawn in by the potential difference across the rock grain surface. This outer layer is called the Gouy layer. The Stern layer is only one ion thick and as shown in Figure 1, the electric potential drops sharply across this layer. Boltzmann distributions can be used to describe the concentrations of ions in the Gouy layer, provided that the electrolytic content in the water is lower than 0.1 moles per liter. The electric potential in this layer of diffused ions is described by the following equation:

$$\varphi(x) = \varphi_0 e^{-kx}$$

Where:

k = inverse Debye radius

x = distance from the charged surface

The slipping plane is the area where relative movement between the solid and water allow for motion between the outer diffused layer of ions and the inner strongly bound ions. This slipping plane has an electric potential across it that is called the zeta (ζ) potential. This electric potential is produced by the shearing between the inner and outer ions of the Stern and Gouy Layers. The Zeta potential plays an important role in the electro kinetic effect and is part of the equation used to determine the electromagnetic coupling tensor, which in turn determines the magnitude of the electromagnetic field induced.

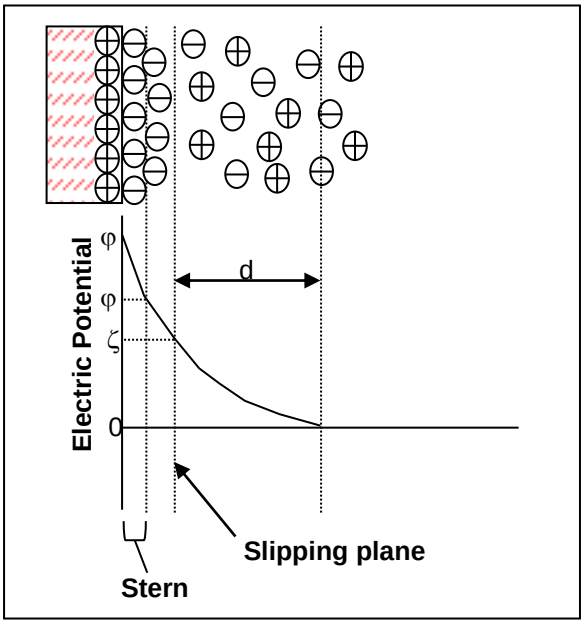

Figure 1 - Electric double layer[6]

1.3 The electro seismic effect[22]

The electro seismic effect can be observed when a fast traveling p wave intersects a water saturated interface of differing anelastic or electrical properties. The electro seismic effect is in effect a form of converted energy which is released as dissipated energy. This conversion of energy takes place when a fast moving P waves produce

slower P waves as it passes through the interface. These slow P waves produce much more movement between the rock and water. This in turn leads to a high loss of energy in the form of heat due to friction and electro seismic effects, such as electromagnetic radiation due to ionic movement. Electro seismic signals are produced by the out of phase motion between all the ions in the water and those attached to the rock. The relationship between applied pressure *P* and electric potential response ϕ for a porous rock is generally given by the following equation (Millar and Clarke 1997)[15]:

$$\phi = -CP = -\left(\frac{\varepsilon\varepsilon_0\zeta}{\eta\sigma}\right)P$$

Where,

ϕ = electrical potential response or streaming potential

C = electro kinetic coefficient

P = applied pressure

$\varepsilon\varepsilon_0$ = permittivity of the pore space

ζ = zeta potential

η = fluid viscosity

σ = electrical conductivity

This equation relates the electrical potential response ϕ developed in a porous rock to the stimulus of an incident pressure change *P*, allowing the rock to be characterised by *C* on a macroscopic scale when modelling such electro kinetic responses. To see how the electro seismic function is derived please refer to Fourie's dissertation on electro-seismic field theory 2000[6].

1.4 Wave Behavior[22]

Du Preez, 2005[22] show a seismic wave propagating in a medium can induce an electrical field or cause radiation of an electromagnetic wave. There are two electro-seismic effects that are considered in this report. The first effect is caused when a seismic wave crosses an interface between two media. When the spherical P-wave crosses the interface, it creates a dipole charge separation due to the imbalance of the streaming as shown in Figure 2. The second effect is caused when a seismic head wave travels along an interface between two media. It creates a charge separation across the interface, which induces an electrical field. This electric field moves along the interface with the head wave and can be detected by antennas when the head wave passes underneath as shown in Figure 3. Currents induced by the seismic wave on opposite sides of the interface. The electrical dipole radiates an EM wave which can be detected by remote antennas

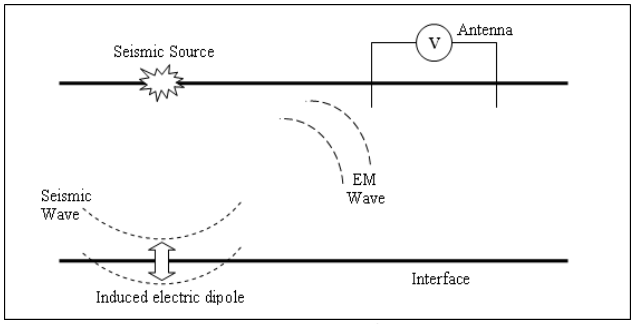

Figure 2 - Seismic wave crossing an interface generating an electromagnetic wave.[22]

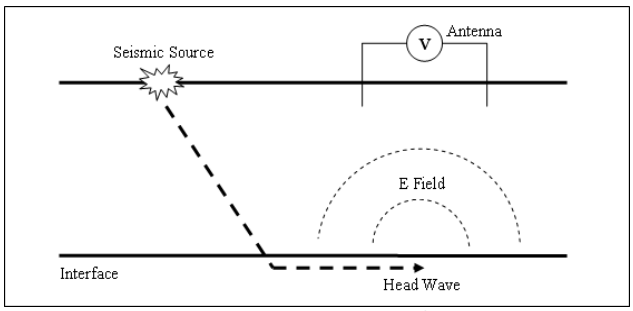

Figure 3 - Head wave travelling along an interface generating an electric field.[22]

2 Site Description

The blind test site chosen for the study, provided by Contact Energy Ltd, is located to the South West of Mt Tauhara within the Tauhara Geothermal System located near the town of Taupo. The Tauhara Geothermal System is currently utilised for geothemal energy and the TH10 geothermal well site is the southern most drilled production capable well in the field. The well is also the second deepest well in the field, at 2326m deep. It is ideally suited to a comparative study of the applicability of electro-seismic geophysical techniques to geothermal systems. This is due to the comprehensive well information available for the site. The survey site consist of twenty two survey points laid out on a grid and analysed as a set of four profiled lines as shown in Figure 4. There are a number of man-made structures on the site indicated on Figure 4. These structures consist of two deep pits and one gravel mound. The presence of these structures dictated

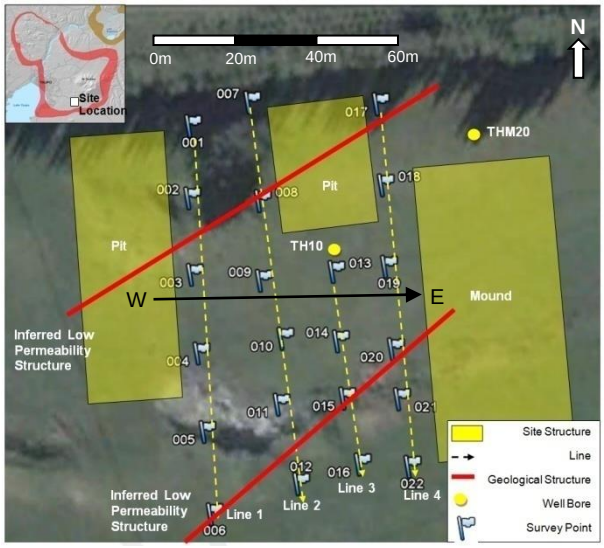

Figure 4 – Site description

the placement of the survey point grid. The points were laid out in order to create four profile lines of 100m length which surround the deep geothermal well TH10 located at the centre of the survey grid. Line 3 was cut short due to the position of the man made pit to the north of the site. The grid size is approximately 100m by 80m and is sufficient for a comparative study. Figure 4 also indicates the position of two inferred geological structures across the site, interpreted from this study. These structures will be discussed later in the study. The TH10 well characteristics are shown in Table 1.

Table 1 - TH10 Well information [21]

Well	TH10
Well Date	13/02/08
Location E (m)	270787.14
Location N (m)	593925.74
Elevation (m)	525
Max measured Depth (m)	2326
True vertical Depth (m)	2326
Cased Depth (m)	973
Casing size (inch)	9 5/8
Liner Depth (m)	2321
Liner size (inch)	7
Well Type	Vertical

3 Site Geology and Lithology[21]

The geology and lithology of the TH10 bore site, provided after the electro seismic interpretation of the TH10 well as presented to Contact Energy, is shown in Table 2 and illustrated on Figure 5. There are a number of geological changes with respect to the geology to the north west of the site which is currently the production area of the Tauhara Geothermal System.

Table2 TH10 Geological and Lithology Log[21]

No	Depth (m)	Formation	Lithology
1	0 to 36	SURFICIAL DEPOSITS	Taupo Formation and post-Oruanui tephra units
2	36 to 82	ORUANUI FORMATION	Massive, pumice-lithic-crystal, coarse ash tuff (non-welded ignimbrite)
3	82 to 84	HUKA FALLS FORMATION	Muddy coarse sandstone and very fine to medium sandstone. Weak smectite, iron oxide and pyrite alteration.
4	84 to 452	CROWBAR RHYOLITE LAVA	Porphyritic rhyolite lava with vitroclastic, spherulitic and flow banded textures. Moderate intensity hydrothermal alteration to clay, iron oxide, calcite, quartz and opaline silica.
5	452 to 512	WAIORA IGNIMBRITE	Vitric-crystal coarse pumiceous tuff. Alteration is moderate to clay, quartz, pyrite and minor calcite, also patchy silicification.
6	512 to 522	RHYOLITE LAVA BRECCIA	Strongly silicified brecciated rhyolite lava. Tubular vesicles and wavy flow banding are common. Phenocrysts include feldspar, quartz and pyroxene. Minor calcite veining is present
7	522 to 1279	WAIORA IGNIMBRITE	Non- to partially- welded ignimbrite flow units. Welding and crystal content fluctuates through the unit. Alteration is intense to quartz, clay, chlorite, epidote, calcite and pyrite.
8	1279 to 1619	LITHIC-CRYSTAL BRECCIA	Lithic and crystal-rich breccia, with crystals of pyroxene, hornblende, feldspar and rare quartz set in a vitric matrix. Lithics of hematite altered porphyritic andesite lava and clay altered tuff lithics are common. Alteration in intense to an assemblage of epidote, clay, chlorite, quartz, minor calcite, pyrite and hematite, and rare wairakite.
9	1619 to 2312	ANDESITE LAVA	Porphyritic andesite lava and breccia with abundant phenocrysts of feldspar and pyroxene with accessory hornblende, set in a recrystallized groundmass. Alteration is intense to epidote, chlorite, clay, quartz, hematite and rare calcite and pyrite.
10	2312 to 2324	TUFFACEOUS SANDSTONE	Tuffaceous sandstone with andesite lava and minor tuff fragments. Alteration is moderate to an assemblage of quartz, illite, chlorite and epidote. Minor veins of quartz and epidote are present.

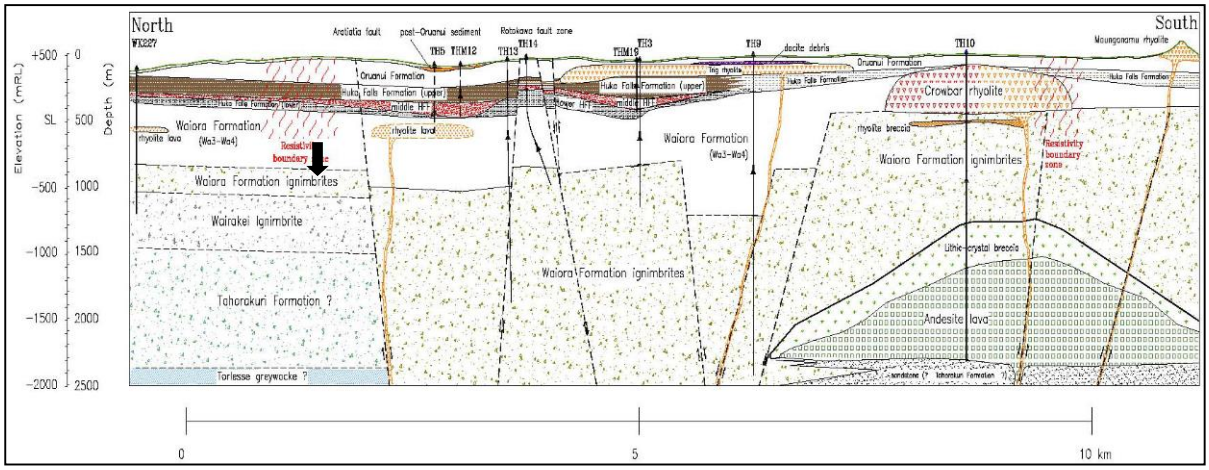

Figure 5 – TH10 and Tauhara Geothermal system geological description[21]

Specifically the Waiora Formation is replaced by the Crowbar rhyolites between 84m to 452m. The Huka Falls Formation between 82m and 84m is also far less significant at the TH10 site than in the wells to the north west. The Waiora ignimbrites start significantly shallower that well logs to the north west of the site indicate. There are also significant andesite lava intrusions at depths of 1619m to 2312m which are absent in well logs to the north west of the site. There is a layer of Tuffaceous Sandstone from 2312m to 2324m which does not appear in any of the other well logs on the Tauhara Geothermal System. The TH10 site is inherently different to the geological structure of the main Tauhara Geothermal System bore field and thus presents an interesting comparative study site.

4 Site Pressure Profile[21]

The TH10 site pressure profile shown on Figure 11 displays a constant pressure gradient from 300m depth to 2300m to of 22 bar to 320 bar.

5 Site Hydrology[21]

The site hydrology is summarised in table 3. There is one major feed at 1900m depth with a steam flow rate of 57 t/h and a number of smaller aquifers from 1000m to 1900m. These known aquifer systems correlate well with the permeability results discussed in section 7.1.

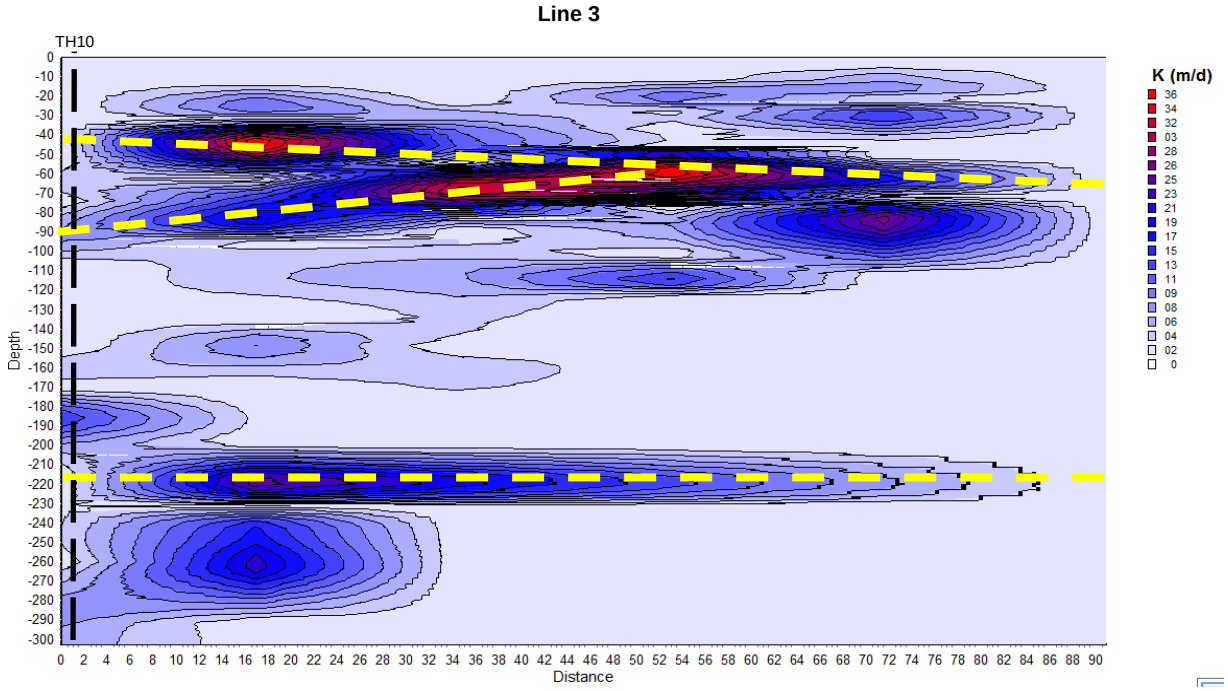

Figure 6 – Shallow Aquifer Permeability analysis (Depth and distance in meters)

Table 3 TH10 Site Hydrology

Depth	Description
95m	Shallow aquifer 60°C
200m	Shallow aquifer 120°C
1000m	Minor deep aquifer feed
1350m	Minor deep aquifer feed
1900m	Major deep aquifer feed
2000m	Minor deep aquifer feed
2100m	Minor deep aquifer feed

The two shallow aquifers at 95 and 200m depth are also heated aquifers. The aquifer at 95m is a steam heated aquifer and the one at 200m is geo-thermally heated.

6 Electro-Seismic Investigation

6.1 Permeability Tomography[22]

Figure 7 shows the electro seismic permeability tomography study results for Lines 1 through 4. The positions and directions of these lines are indicated on Figure 4. The permeability is represented as hydraulic conductivity and expressed in meters per day. The values range from 7.5m/d to 9.5m/d. Figure 6 shows the shallow aquifer interpretation of permeability. Figure 7 also shows the relative position of the TH10 well when looking at the site from west to east as illustrated on Figure 4. This will allow the reader to visualise the aquifers with respect to the TH10 well, as the discussion of results interpret the results from a TH10 well point of view. The major formation changes are also shown on Figure 7. The corresponding formation number is given in accordance with Table 2.

6.2 Electro Seismic Coupling Coefficient Tomography[22]

Figure 8 shows the electro seismic coupling coefficient tomography data for lines 1 through 4. The ESCCT data is representative of the electrical characteristics that define the interaction between the pressure wave to electrical field conversion. The ESCCT data is expressed as a percentage of conversion. In geothermal systems, the electrical characteristics of the aquifer fluids dominate the conversion. Therefore in this study, the high response values are indicative of geothermal aquifer systems with high temperature and high fluid conductivity. Figure 8 also shows the relative position of the TH10 well when looking at the site from west to east as illustrated on Figure 4. This will allow the reader to visualise the aquifers with respect to the TH10 well, as the discussion of results interpret the results from a TH10 well point of view. The major formation changes are also shown on Figure 8. The corresponding formation number is given in accordance with Table 2.

6.3 Fracture Analysis[22]

The fracture analysis tomography results shown in Figure 9 for lines 1 through 4 show the inferred fracture zone depths. The electro seismic data is spectrally analysed and specific frequency patterns associated with fracturing are used to infer fracturing with depth. The results shown in Figure 9 are used to show secondary permeability within a primary permeability aquifer. These fractured zones are associated with higher fluid flow rates. Figure 9 also shows the relative position of the TH10 well when looking at the site from west to east as illustrated on Figure 4. This will allow the reader to visualise the aquifers with respect to the TH10 well, as the discussion of results interpret the results from a TH10 well point of view. The major formation changes are also shown on Figure 9. The corresponding formation number is given in accordance with Table 2.

6.4 Interface Tomography[22]

Interface tomography shown for lines 1 through 4 in Figure 10 indicate the positions of interfaces between rocks or formations with different electrical resistivity. It makes use of the interface effects generated by electro seismic responses as the pressure wave passes through a rock resistive interface. This data can be used to determine if there are large geological shifts such as faults. Furthermore, the interface tomography results indicate positive and negative interface changes illustrated as red and blue respectively on Figure 10. Interface response polarities indicate the type of fluids and rock involved in the generation ES response. Similar rock types generate similar polarity responses thus indicating stratification boundaries. This is very useful in determining which formations the geothermal responses occur in. Figure 10 also shows the relative position of the TH10 well when looking at the site from west to east as illustrated on Figure 4. This will allow the reader to visualise the aquifers with respect to the TH10 well, as the discussion of results interpret the results from a TH10 well point of view. The major formation changes are also shown on Figure 10. The corresponding formation number is given in accordance with Table 2.

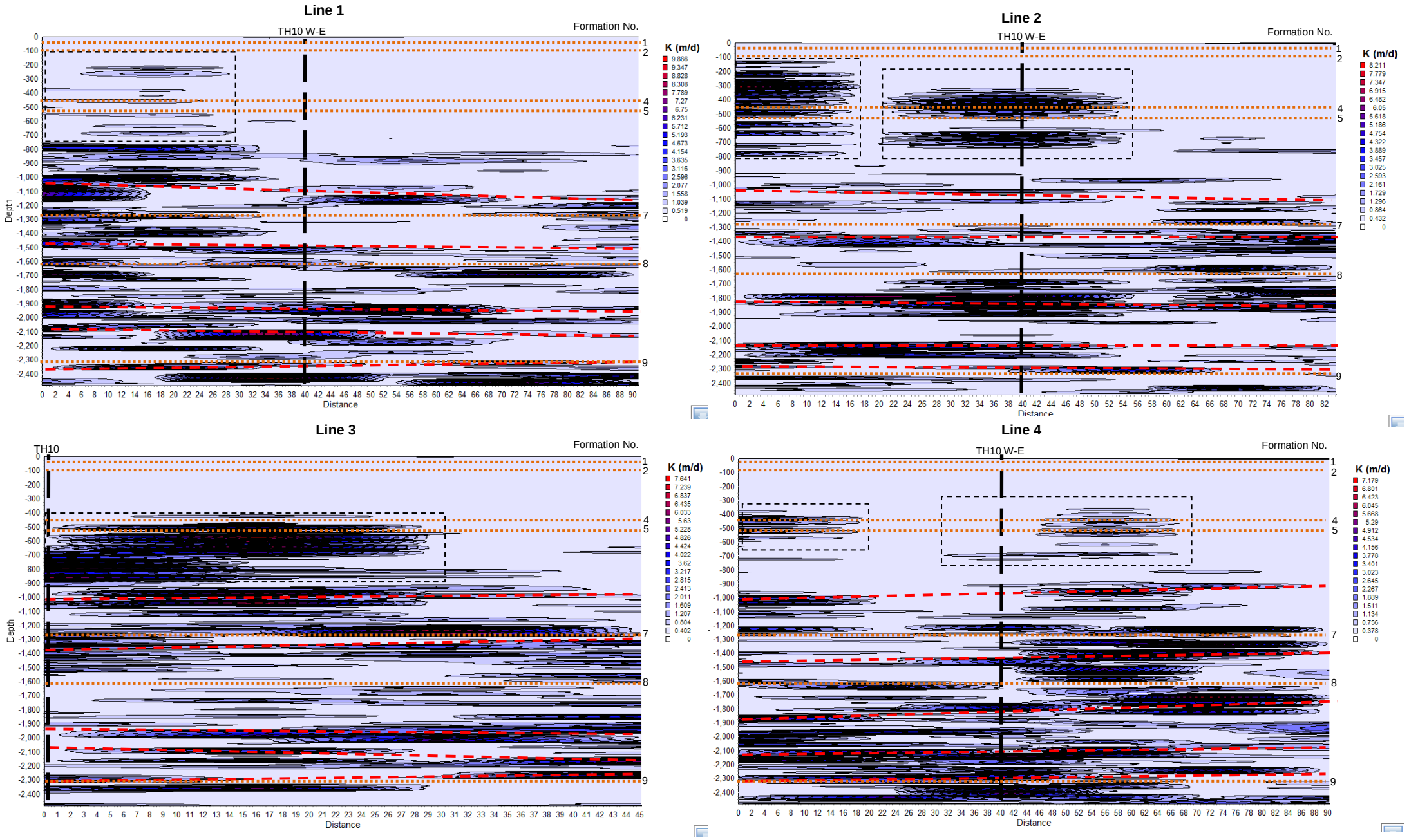

Figure 7 – Deep Aquifer Permeability analysis (Depth and distance in meters)

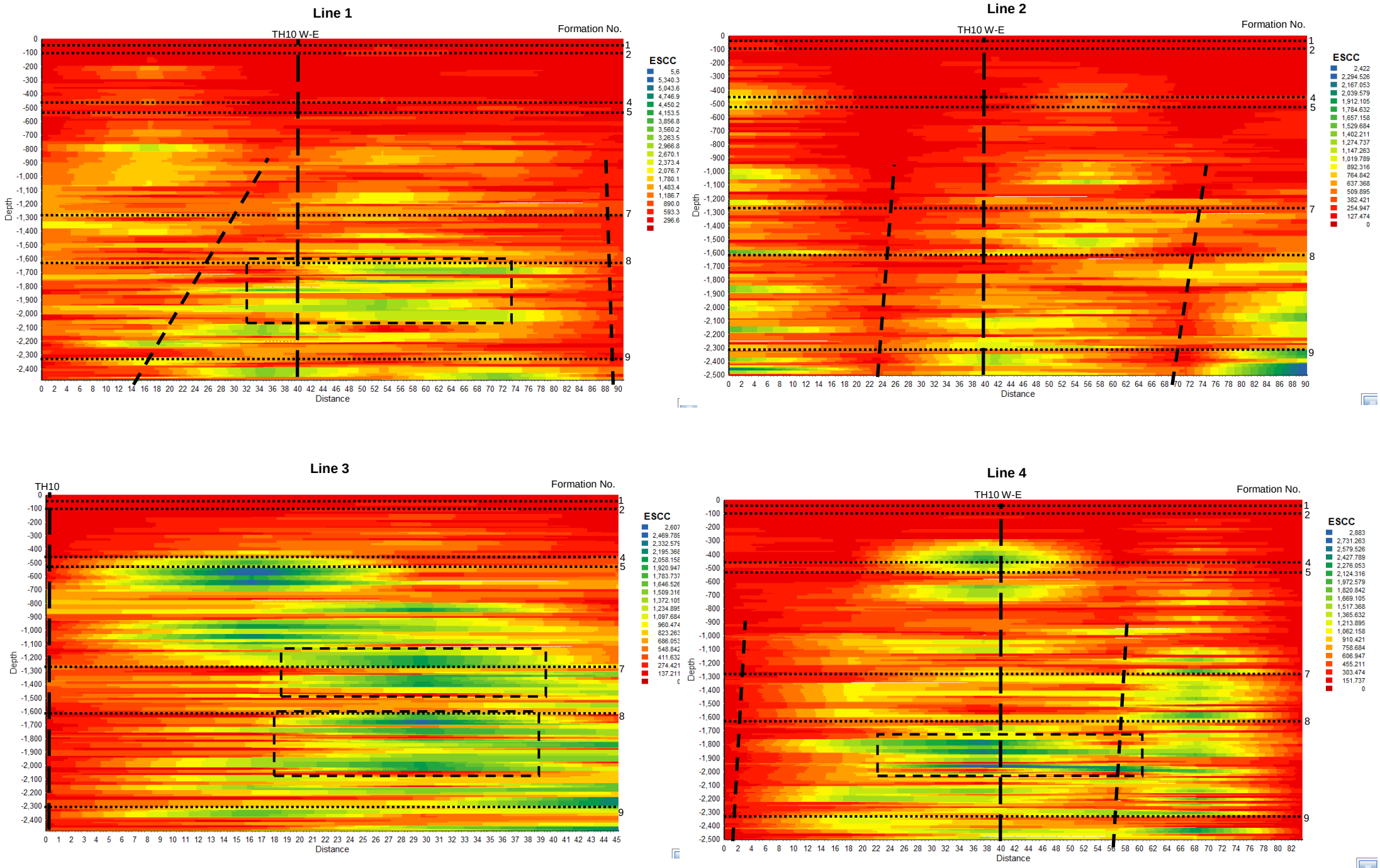

Figure 8 – Deep Aquifer Electro Seismic Coupling Coefficient analysis (Depth and distance in meters)

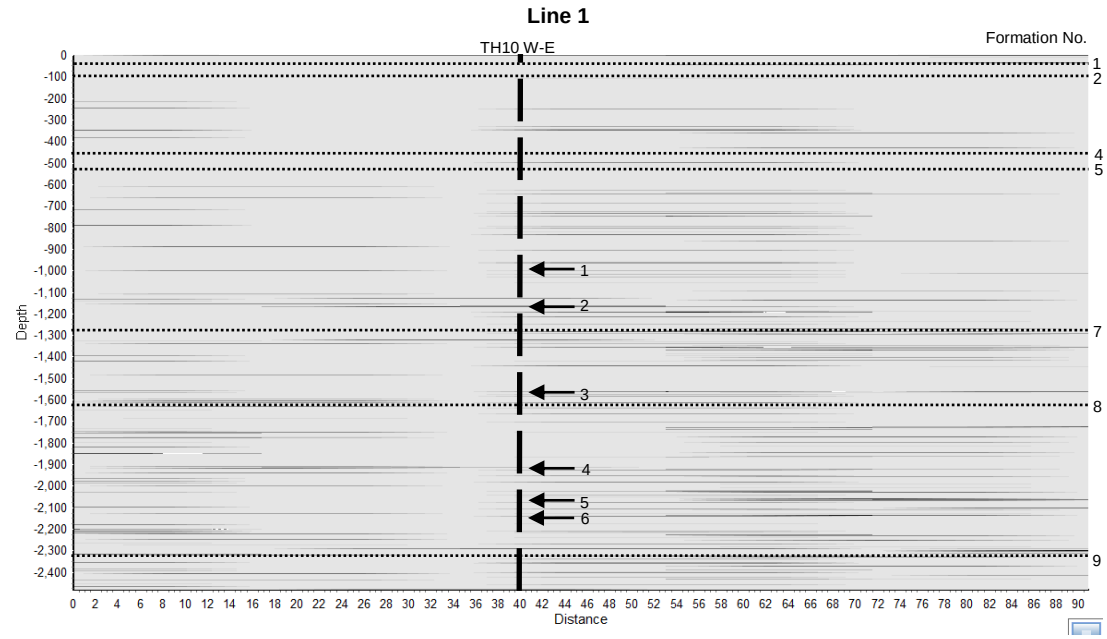

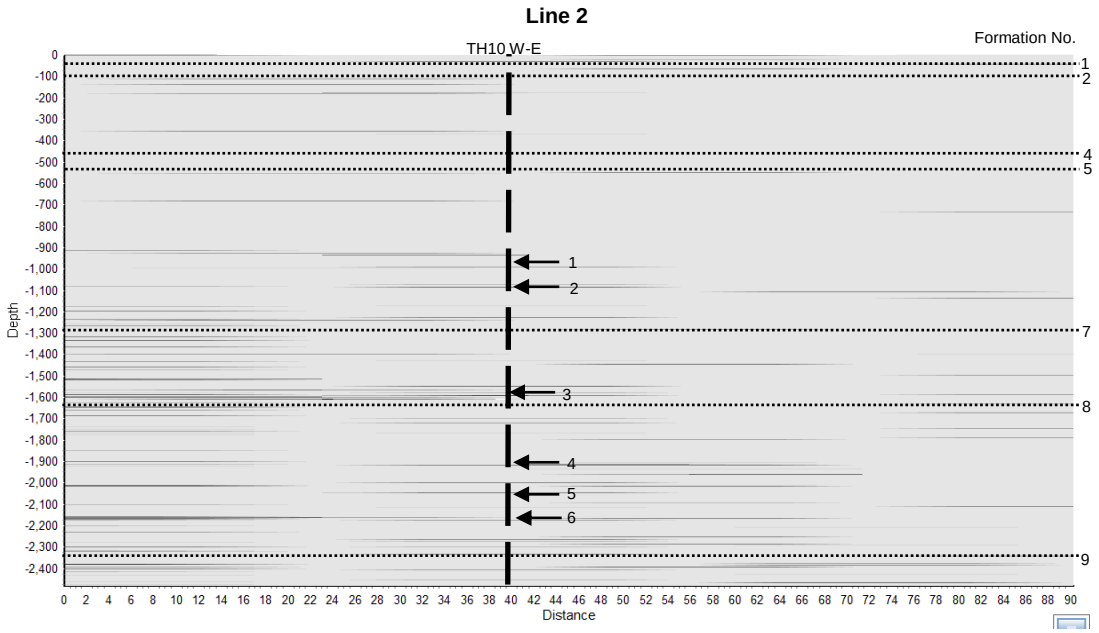

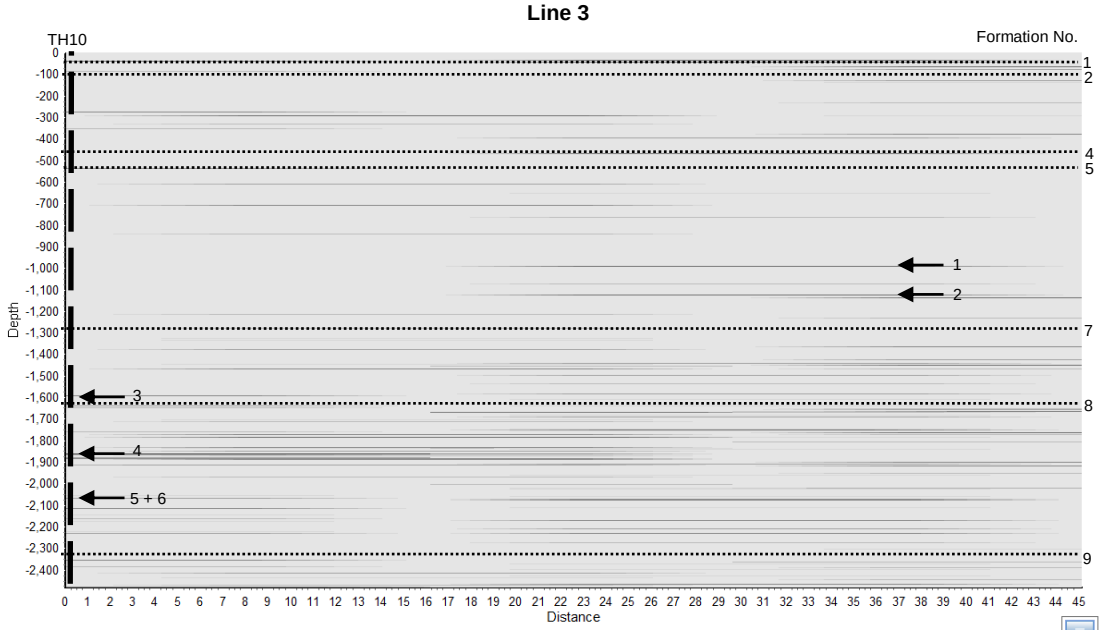

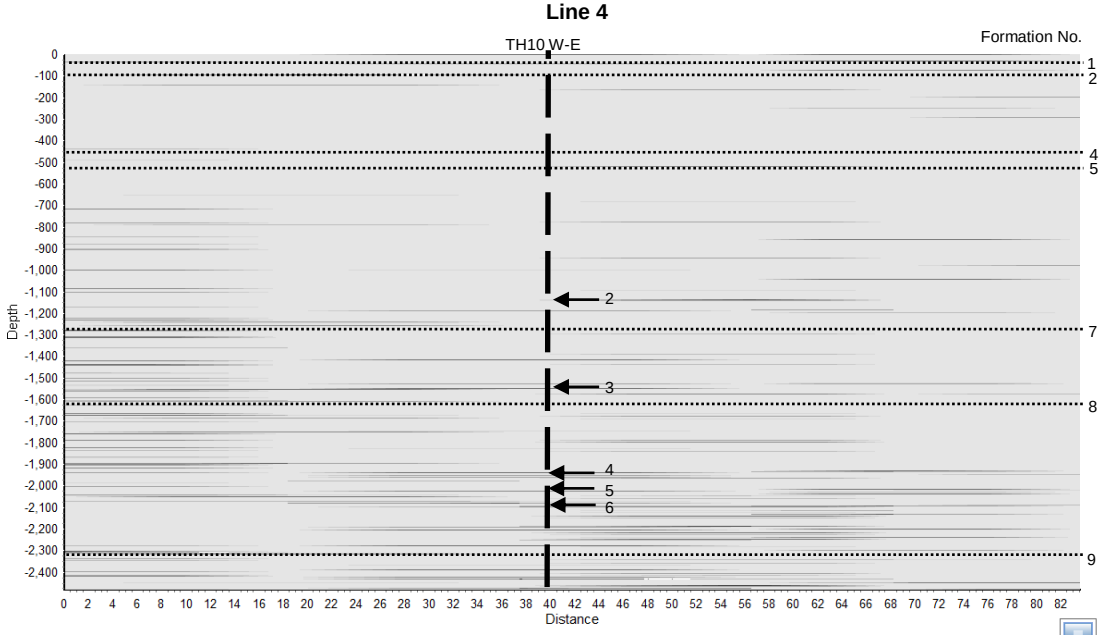

Figure 9 –Fracture analysis (Depth and distance in meters)

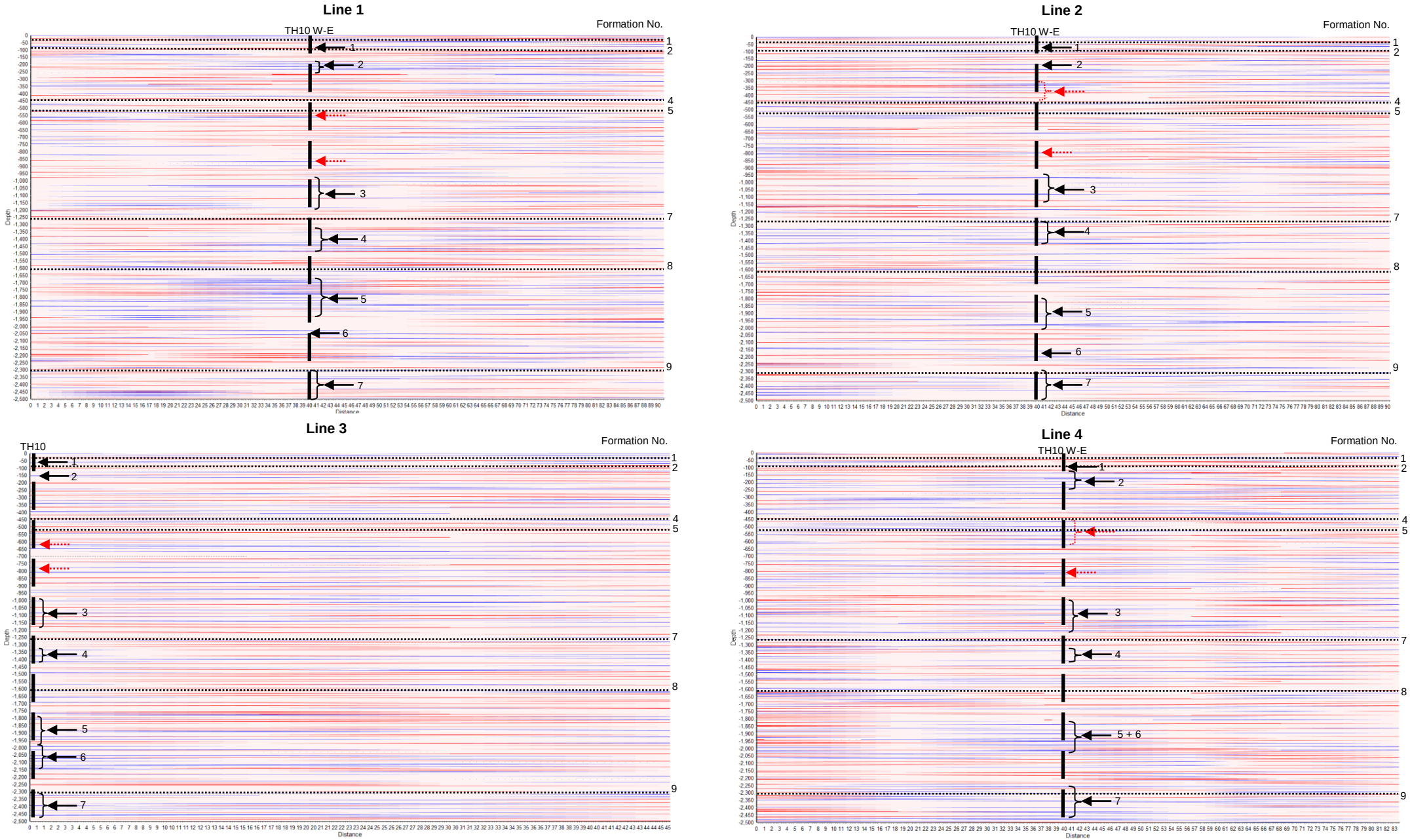

Figure 10 – Interface analysis (Depth and distance in meters)

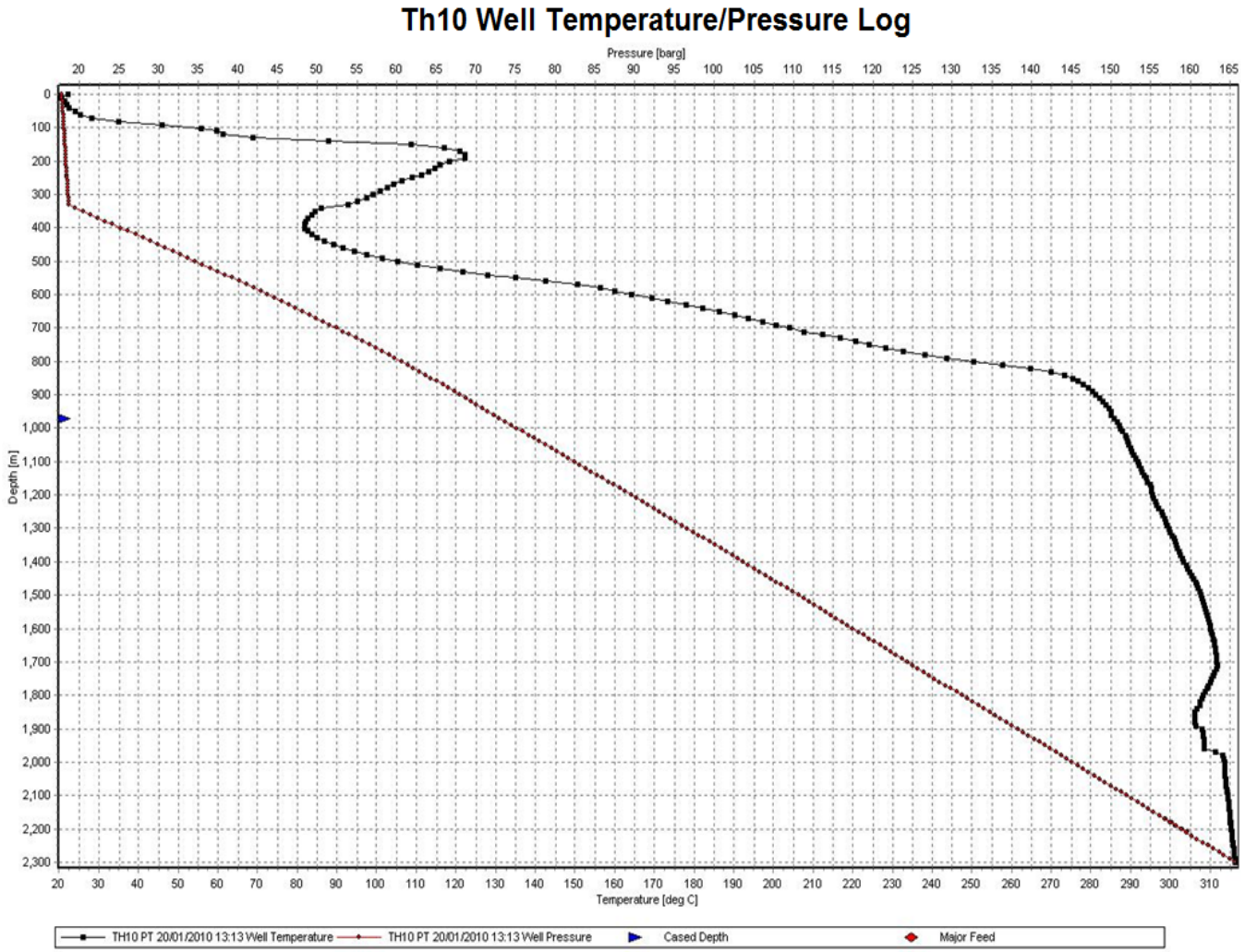

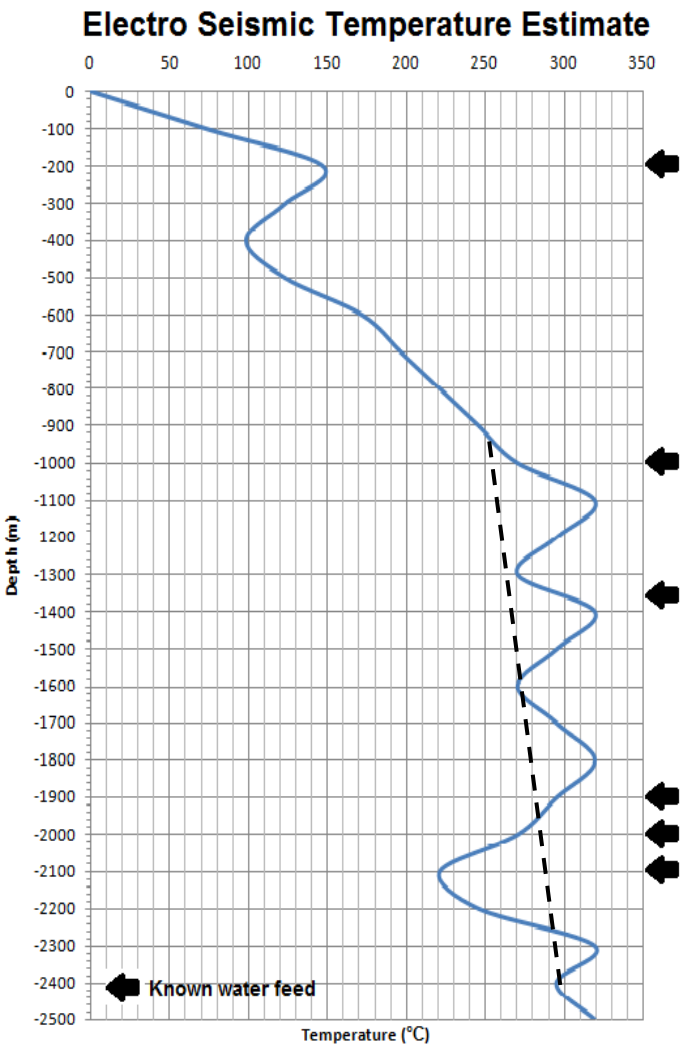

Figure 11 – Electro seismic Temperature estimate to TH10 well Temperature Pressure log comparison

7 Discussion of results

7.1 Permeability Results

The results of the permeability analysis for lines 1 – 4, shown in Figure 7, indicate the presence of deep aquifer systems at approximately 1000m, 1400m and 1800m to 1900m depth. All of these aquifers run across the test site and are therefore considered to have considerable lateral extent. There may be small variations on these depths due to slight seismic velocity variations on each survey point on the site. There are also smaller permeable zones between these distinct aquifer systems indicating relatively high permeability between 1000m and 2500m depth. The known aquifer at 2000m seems to have blended in with the one at 1900m and is not clearly defined in Figure 7. There are also high permeability pockets at 400m and 600m depth that seem to be connected laterally across the site indicating the presence of a highly localised aquifer at these depths. These aquifers are not high flow aquifers as supported by the lack of secondary permeability shown in the fracture analysis in Figure 9. An alternative hypothesis on the existence of these localised anomalies is that the Waiora formation contains a large amount of quartz due to geothermal alteration. Quartz produce streaming potentials when deformed by a pressure wave. As such the highly localised ES responses at 400m and 600m may indicate the positions of high content quartz rock formations. The deeper permeable zones correlate well with the TH10 well logs and known feeds. The aquifers are shown to have permeability between 9.5m/d to 7.5m/d. These values are calibrated against the flow rates known for the TH10 well. The shallow aquifer permeability analysis of line 3, shown in Figure 6, shows two distinct aquifers at 45m, 90m and 210m. This correlates well with the known positions of the shallow aquifers intersecting the site. The aquifers at 45m and 90m lie in course pumice and are shown to be connected in Figure 6. This is not uncommon as pumice is highly porous and permeable. The known formation change positions are also indicated on Figure 7 for lines 1 – 4. There are a number of smaller permeable zones associated with these changes, notably for formation group change 7 and 8 at 1279m and 1619m depth, as indicated on Figure 7. The change at 1619m depth is especially prominent as there is a change from lithic-crystal breccia formation to andesite lava formation. The intrusive lavas may have caused fracturing at this depth which facilitates permeability. This is supported by the fracture analysis discussed in Section 7.3.

Table 3 shows the correlation between the known aquifers in the TH10 well and the electro seismically interpreted depths estimated for this study. As shown, the interpreted aquifers at 400m and 600m are not represented in the actual well logs. The aquifer at 2000m is not clearly discernable from the interpreted aquifer at 1900m and as such is not interpreted as an individual aquifer on the table.

Table 3 TH10 Site Comparative Hydrology

Known TH10 Aquifer Depths	ES Estimated Aquifer Depths
95m	45m to 90m
200m	210m
Possible piezo electric response	400m
Possible piezo electric response	600m
1000m	1000m
1350m	1400m
1900m	1800m to 1900m
2000m	Indiscernible from aquifer at 1900m
2100m	2100m
Below TH10 drill depth	2350m

7.2 Electro Seismic Coupling Coefficient Results

The ESCCT results show the presence of high temperature geothermal reservoirs from 1000m to 2500m depth on all of the lines. There is also a shallow resource at approximately 400m depth which is also present in the permeability analysis. The strongest responses come from the reservoirs at 1800m and 1900m depth. There are slightly weaker reservoirs at 1300m to 1400m and 1000m to 1100m. These distinct geothermal active areas are clearly defined by zones of low ES response. This indicates that they are not connected beneath the study site and are separate aquifers that supply independent flow. There are two regions that intersect the site with a distinct low ESCCT response. These areas of low response are clearly visible on Figure 8 and shown on the site map on Figure 4. The reason for these low responses are unknown, however they indicate a change of fluid rock interaction and may be associated with a different intrusive rock formation however this is not certain. The TH10 well is positioned at the border of one of the low response zones as indicated on Line 3 of Figure 8. This may be the reason that the TH10 well has a lower flow rate than some of the production wells in the geothermal field. The areas of highest ESCCT response are also shown on Figure 8. These zones are at approximately 1300m and 1900m depth which correlate well with the known production depths for the TH10 well. This correlation indicates a strong connection between ESCCT response and geothermal activity measured for TH10. There is also a high response in the permeable areas at 400m and 600m.

However they do not seem to have a great deal of flow contribution in the Th10 well. This may be due to the fact that these aquifers appear to be highly localised and may not have the ability to provide sufficient flow into the well. The formation change boundaries indicated in Figure 8 are associated with low ES response and clearly define the geothermal resource boundaries.

7.3 Fracture Analysis Results

The fracture analysis shown in Figure 9 shows a great deal of fracturing from 1000m to 2500m on all of the lines. The six main fracturing groups that show in all the lines are indicated on Figure 9. The groups with the strongest degree of fracturing are groups 3 and 4 at depths 1600m and 1900m respectively. Group 4 at depth 1900m indicates a high degree of secondary permeability in the aquifer at 1900m as shown in Table 3. This strongly correlates with the known main feed in TH10 at 1900m. This is also supported by the permeability data which shows high primary permeability for the aquifer at 1900m and the ESCCT data that indicates a strong geothermal resource at 1900m depth. It is generally accepted that secondary permeability produced by fracturing in the rock formation facilitates high fluid or gas flow within the rock formation. There is also, to a lesser degree, fracturing in groups 1 and 2 at 1000m and 1100m depths respectively. These fractures may be providing TH10 with higher permeability at these depths, facilitating flow to the well. This is also true for Groups 5 and 6 at depth 2000m and 2100m which show some fracturing and also improve permeability at these depths. The fracture group 3 at 1600m indicates a high degree of secondary permeability; however, there is very little primary permeability at this depth. This may be why there is no indication of actual flow in the TH10 well at this depth. There is however a change in formation at this depth from the Lithic-Crystal Breccia Formation to the Andersite Lava Formation. Fracturing could be occurring at this formation interface. A summary table of the Known TH10 well feeds to the ES fracture depth estimates are shown in Table 4.

Table 4 ES fracture estimates to known TH10 feed comparison

ES fracture Depth Estimate	Known TH10 Feed Depths
1000m	1000m
1100m	1100m
1600m	Formation change
1900m	1900m
2000m	2000m
2100m	2100m
2320m	Formation change

7.4 Interface Tomography Results

The ESIT results are shown on Figure 10. The results of the interface tomography indicate that the geology under the TH10 test site is highly stratified and shows no indication of major faulting. The interface polarity data indicates that the interfaces associated with geothermally active formations are negative in response, as illustrated by the blue traces. The negative ESIT data is broken into 7 formation depth groups as illustrated on Figure 10. Groups 1 and 2 show the formations that hold the upper two geothermally heated aquifers. Group 3 shows the formation that holds the first deep geothermal aquifer at 1000m to 1100m. Group 3 indicates that the two known aquifers are a part of the same formation and share heat resources. This correlates well with the known feeds at 1000m and 1100m depth in the TH10 well. Group 4 indicates an independent geothermal resource at 1300m to 1400m depth. This correlates well with the known feed at 1350m depth in the TH10 well. Groups 5 and 6 indicates partially connected geothermal formations from 1800m to 2100m. At the TH10 well they are separated by a non permeable layer however on line 4 the non permeable layer is not as prominent and the two formations may be hydro-thermically connected. These groups correlate very well with the known TH10 well feeds at 1900m, 2000m and 2100m. The ESIT data indicates that these aquifers share the same geothermal formation resource and are merely high permeability flow paths within this shared geothermal formation. Group 7 indicates an independent deep geothermal formation at 2300m to 2500m depth, under the TH10 well. This is not confirmed as the TH10 well was not drilled to these depths. It does infer deeper geothermal resources under the TH10 well. The red pointers in Figure 10 show the positions of interpreted geothermal formations at 400m and 600m that do not correlate with the TH10 well log data. As discussed before, they do not seem to have a great deal of flow contribution in the Th10 well. This may be due to the fact that these aquifers appear to be highly localised and may not have the ability to provide sufficient flow into the well. They may also indicate the presence of high quartz content rock which is also capable of producing ES responses through piezo electric effects. These piezo electric effects may also produce negative interface responses as indicated in Figure 10. The andersite lava formation defined by Group 9 produces the most geothermal ES interface response which is confirmed by the temperature log illustrated in Figure 11. Table 5 shows a summary of the major ESIT geothermal formation depth estimates compared to the TH10 well log data.

Table 5 ESIT geothermal formation interpretations compared to the TH10 well log data.

Group	ES Estimate	TH10 Well Log
1	100m	95m
2	180m – 220m	200m
3	1000m – 1100m	1000m and 1100m
4	1300m – 1400m	1350m
5	1800m – 1950m	1900m
6	2000m – 2150m	2000m and 2100m
7	2300m – 2500m	Below TH10 drill depth
-	400m	Possible piezo electric response
-	600m	Possible piezo electric response

7.5 Electro Seismic Temperature Estimation Tomography Results

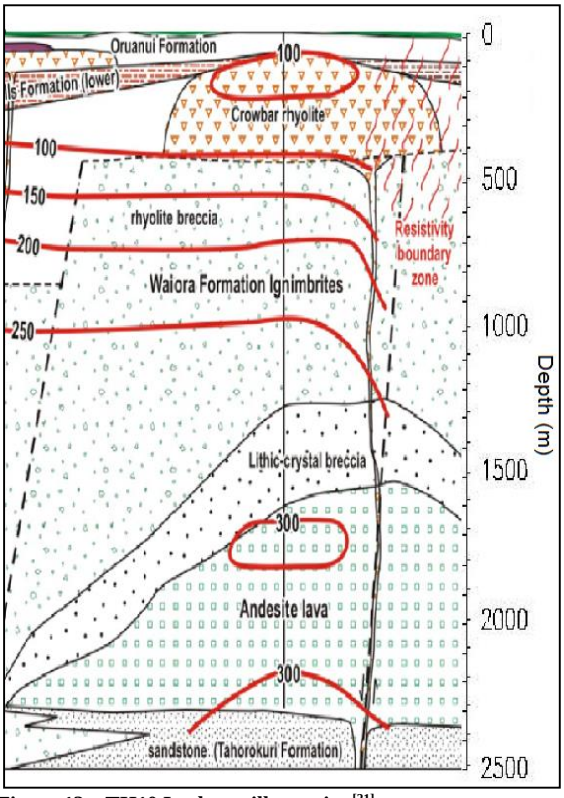

Figure 12 – TH10 Isotherm illustration[21]

The TH10 well temperature-depth data is shown in Figure 11. There is a distinct temperature increase at 200m depth of 120°C which is representative of cross flow above the Crowbar Rhyolite formation which is considered to be feeding the warm water at Waipahini. The temperatures of 300°C below 1000m depth is also thought to be due to the proximity of a deep up flow zone to the South of Mt Tauhara. The Waipahini outflow water are derived by dilution of deep up-flow fluids with cool meteoric groundwater which further supports the cross flow model thought to exist at the TH10 site. The TH10 site has one of the highest temperatures, 300°C, in the Tauhara Geothermal system. There is also a temperature fluctation between 1700m to 2000m depth indicating the presence of a deep permeable flow zone. After the site information was released by Contact Energy, a temperature estimate algorythm was developed to predict the temperature gradients for the TH10 well. The right graph on Figure 11 shows the temperature estimate generated from the electro seismic data recorded for line three. The data is calibrated to 320°C at 2300m depth. There is a stong correlation between the well log temperature and the electro siesmic temperature estimate data. The temperature increase at 200m depth shows clearly on the estimate graph, however it is estimated to be 30°C higher in temperature than actual temperature of 120°C. The temperature increase from 400m to 900m also correlated well with estimate log. The depth posistions of the known aquifer feeds are shown on the estimate graph. The depths of these aquifers strongly correlate with the peaks on the electro seismic temperature estimate. This indicates that high permeability affects the temperature estimate by overestimating the temperatures at these high permeability zones. This is true for the aquifer at 200m that is over estimated by 30°C. To show a more representative temperature gradient for the estimate, the temperature at low permeabilities zones are taken as the average temperature. This was done for the depths between 900m and 2500m and illustrated on Figure 11. This temperature gradient is more representative of the actual temperature. Figure 12 shows the isotherms for TH10 and its surrounding area. A linear gradient is estimated for the field that sharply varies toward the geothermal feild resistive boundry.

8 Conclusions

This comparative study demonstrates that the electro seismic permeability tomography, ESCCT, ESFT, ESIT and ES temperature estimate geophysical methods show good correlation with the TH10 geological, lithological, temperature, pressure and flow well logs. Although a great deal more study and testing is required to refine electro seismic methods and techniques, this study indicates that the electro seismic method can be used to effectively delineate and map geothermal resources, permeability, fracturing and geological interfaces. The ES temperature estimation method also shows potential at mapping hot rock formations for enhanced geothermal systems, however this method also needs to be tested further.

9 Acknowledgements

This comparive study would not have been possible without the assistance of Contact Energy Ltd, New Zealand, who provided site access to the TH10 well as well as supporting geological, lithological, hydrological temperature and pressure data for the TH10 well.

10 References

1. Biot, M. A. (1956) Theory of propagation of elastic waves in a fluid-saturated porous solid. I. Low frequency range. *Journal of the Acoustical Society of America.*

2. Biot, M. A. (1956) Theory of propagation of elastic waves in a fluid-saturated porous solid. II. Higher frequency range. *Journal of the Acoustical Society of America.*

3. Biot, M. A. (1962) Generalized theory of acoustic propagation in porous dissipative media. *Journal of the Acoustical Society of America.*

4. Botha, J. F., Verwey, J. P., Van der Voort, I., Vivier, J. J. P., Colliston, W. P. and Loock, J. C. (1998) *Karoo Aquifers. Their Geology, Geometry and Physical Behaviour*. Water Research Commission.

5. Butler, K. E., Russell, R. D. and Kepic, A. W. (1996) Measurement of the seismoelectric response from a shallow boundary. *Geophysics.*

6. Fourie, F. D. (2000) *An Introduction to Geophysics for Geohydrologists*. Unpublished lecture notes. Institute for Groundwater Studies, University of the Orange Free State.

7. Garambois, S. and Dietrich, M. (2001) Seismo-electric wave conversion in porous media: Field measurements and transfer function analysis. *Geophysics.*

8. Haartsen, M. W. and Pride, S. R. (1997) Electroseismic waves from point sources in layered media. *Journal of Geophysical Research.*

9. Haartsen, M. W., Dong, W. and Toksöz, M. N. (1998) Dynamic streaming currents from seismic point sources in homogeneous poroelastic media. *Geophysical Journal International.*

10. Ishido, T. (1981) Experimental and theoretical basis of electrokinetic phenomena in rockwater systems and its application to Geophysics. *Journal of Geophysical Research.*

11. Kepic, A. W., Maxwell, M. and Russell, R. D. (1995) Field trials of a seismoelectric method for detecting massive sulphides. *Geopysics.*

12. Martner, S. T. and Sparks, N. R. (1959) The electroseismic effect. *Geophysics.*

13. Maxwell, M., Russell, R. D., Kepic, A. W. and Butler, K. E. (1992) Electromagnetic responses from seismically excited targets B: Non-piezoelectric phenomena. *Exploration geophysics.*

14. Mikhailov, O. V., Haartsen, M. W. and Toksöz, M. N. (1997) Electroseismic investigation of the shallow subsurface: Field measurements and numerical modelling. *Geophysics.*

15. Millar, J. W. A. and Clarke, R. H. (1997) *Electrokinetic techniques for hydrogeological site investigations*. Groundflow

16. Pride, S. R. (1994) Governing equations for the coupled electromagnetics and acoustics of porous media.

17. Pride, S. R. and Haartsen, M. W. (1996) Electroseismic wave properties. *Journal of the* Acoustical Society of America.

18. Pride, S. R. and Morgan, F. D. (1991) Electrokinetic dissipation induced by seismic waves. Geophysics.

19. Ranada Shaw, A., Denneman, A. I. M. and Wapenaar, C. P. A. (2000) Porosity and permeability effects on seismo-electric reflection. In: Proceedings of the EAGE conference.

20. Russell, R. D., Butler, K. E., Kepic, A. W. and Maxwell, M. (1997) Seismoelectric exploration. The Leading Edge.

21. Rosenberg, M., Wallin, E., Bannister, S., Bourguigon, S., Jolly, G., Mroczek, E., Milicich, S., Graham, D., Bromley, C., Reeves, R., Bixley, P., Clothworthy, A., Carey, B., Climo, M. (2010) Tauhara Stage || Geothermal Project: Geoscience Report, GNS Science Consultancy Report 2010/138.

22. Du Preez, M. (2005) Accuracy of Electro-Seismic Techniques Applied to Groundwater Investigations in Karoo Formations. Master Thesis: University of the Free State

23 Frenkel, J. (1944) On the theory of seismic and seismoelectric phenomena in moist soil. *Journal of Physics (Soviet).* 230-241.

24 Biot, M. A. (1956a) Theory of propagation of elastic waves in a fluid-saturated porous solid. I. Low frequency range. *Journal of the Acoustical Society of America.* **28** (2), 168–178.

25 Biot, M. A. (1956b) Theory of propagation of elastic waves in a fluid-saturated porous solid. II. Higher frequency range. *Journal of the Acoustical Society of America.* **28** (2), 179-191.

26 Biot, M. A. (1962a) Generalized theory of acoustic propagation in porous dissipative media. *Journal of the Acoustical Society of America.* **34** (9), 1254-1264.

27 Biot, M. A. (1962b) Mechanics of deformation and acoustic propagation in porous media. *Journal of Applied Physics.* **33** (4), 1482-1498.

28 Chandler, R. (1981), Transient streaming potential measurements on fluidsaturated porous structures: An experimental verification of Biot's slow wave in the quasi-static limit, *J. Acoust. Soc. Am.*, *70*, 116–121.